DOI: 10.6060/mhc245862b

Effect of the Synthesis Technique on the Structure of Tetrafluorosubstituted Tin Phthalocyanines

Darya D. Klyamer,[a] Aleksandr S. Sukhikh,[a] Dmitry V. Bonegardt,[a] Dmitriy N. Polovyanenko,[b] and Tamara V. Basova[a@]

[a]*Nikolaev Institute of Inorganic Chemistry, Siberian Branch of Russian Academy of Sciences, 630090 Novosibirsk, Russia*
[b]*N.N. Vorozhtsov Novosibirsk Institute of Organic Chemistry, Siberian Branch of Russian Academy of Sciences, 630090 Novosibirsk, Russia*
[@]*Corresponding author E-mail: basova@niic.nsc.ru*

Dedicated to the memory of Academician Oskar Iosifovich Koifman

In this work, we demonstrate the effect of the synthesis technique on the structure of tetrafluorosubstituted tin phthalocyanines. Tetrafluorinated phthalocyanines of tin(II) and tin(IV) with substituents in peripheral and non-peripheral positions were synthesized by two different techniques, namely by fusing fluorinated phthalonitriles with $SnCl_2$ and refluxing of the initial reagents in 1-chloronaphthalene, as a result of which their single crystals were grown and the crystal structure was determined. It was shown that during synthesis by the first technique, $Sn(II)PcF_4$ complexes were formed. At the same time, during the synthesis by the second technique, complexes of Sn(IV), namely $Sn(IV)Cl_2PcF_4$, were formed. Thin films of $Sn(II)PcF_4$ deposited by vacuum sublimation were also investigated by an X-ray diffraction method.

Keywords: Tin(II) phthalocyanines, tin(IV) phthalocyanines, fluorinated phthalocyanines, crystal structure, thin films.

Влияние метода синтеза на структуру тетрафторзамещенных фталоцианинов олова

Д. Д. Клямер,[a] А. С. Сухих,[a] Д. В. Бонегардт,[a] Д. Н. Половяненко,[b] Т. В. Басова[a@]

[a]*Институт неорганической химии им. А.В. Николаева СО РАН, 630090 Новосибирск, Россия*
[b]*Новосибирский Институт органической химии им. Н.Н. Ворожцова СО РАН, 630090 Новосибирск, Россия*
[@]*E-mail: basova@niic.nsc.ru*

Посвящается памяти Академика РАН Оскара Иосифовича Койфмана

В данной работе показано влияние метода синтеза на структуру тетрафторзамещенных фталоцианинов олова. Тетрафторированные фталоцианины олова(II) и олова(IV) с заместителями в периферийном и непериферийном положениях были синтезированы двумя различными методами, а именно сплавлением фторированных фталонитрилов с $SnCl_2$ и кипячением исходных реагентов в 1-хлорнафталине, были выращены их монокристаллы и определена кристаллическая структура. Было показано, что при синтезе в расплаве образуются комплексы $Sn(II)PcF_4$, а при синтезе в среде 1-хлорнафталина образуются комплексы Sn(IV), а именно $Sn(IV)Cl_2PcF_4$. Кроме того тонкие пленки $Sn(II)PcF_4$, полученные методом вакуумной сублимации, были исследованы методом рентгеновской дифракции.

Ключевые слова: Фталоцианины олова(II), фталоцианины олова(IV), фторированные фталоцианины, кристаллическая структура, тонкие пленки.

Introduction

Among other molecular organometallic compounds, metal phthalocyanines have a number of advantages, such as high chemical and thermal stability, as well as a variety of methods for the deposition of ordered thin films on various substrates. Most phthalocyanine complexes have flat geometry but phthalocyanines with some metal cations, *e.g.* Pb(II) and Sn(II), have a saucer-shaped structure. In addition, phthalocyanines of Sn(IV), Si(IV), Ge(IV), Zr(IV), Al(III), Ga(III), In(III), Fe(III) and Bi(III) can attach ligands to axial positions, which also leads to a distortion of the planar geometry of the macrocycle.[1–3] Due to the special arrangement of molecular stacks and the π-π overlap of neighbouring macrocycles, nonplanar phthalocyanines demonstrate enormous potential for many applications, for example, in organic photovoltaics and field effect transistors.[4–7]

Tin(II) phthalocyanine (Sn(II)Pc) is one of the representatives of phthalocyanines with a saucer-shaped structure, which is widely used in catalysis,[8] solar cell elements,[9] optical and chemiresistive sensors.[10] The crystal structure of Sn(II)Pc has been determined by Mason *et al.*[11] and then by Kubiak *et al*.[12] It crystallizes in the triclinic system with a P1 space group (Z=2). It is known that in monolayers or in ultrathin films consisting of several monolayers on Sn(II)Pc may have different flat-lying geometries defined by the position of a tin atom protruding from the macrocycle ("Sn-up" and "Sn-down") depending on the type of substrates (Au, TiO_2, FeO, *etc*.), deposition conditions and post-deposition annealing.[13,14] The synthesis and properties of some Sn(II)Pc bearing various substituents, *e.g.* NO_2,[15] SO_3H-[16] 2,3-dihydro-1H-inden-5-oxy,[17] 2,6-dimethoxyphenoxy,[18] dodecyl-mercapto,[19] *etc*., were also described in the literature. At the same time, fluorinated tin(II) phthalocyanine derivatives were not investigated.

Sn(IV)Pc complexes, which can bind two axial ligands are also well known and of great interest because axial ligands prevent aggregation due to stericity on each side of the ring.[20,21] For example, $SnPcCl_2$ without substituents in the macroring and its thin films were studied in detail,[22,23] and it was found that it crystallizes in two crystal phases (monoclinic and triclinic).[21,24] Similarly to Sn(II)Pc,[25] Sn(IV)$PcCl_2$ can be sublimed in a vacuum with the formation of polycrystalline thin films.[23] The structural evolution of $SnCl_2Pc$ films grown by thermal evaporation on various substrates and their application in field effect transistors were studied in the cycle of works by Giri with co-authors.[26–28]

Tin(IV) chloride phthalocyanines with 4-*tert*-butylphenoxy,[29] 2,6-dimethoxyphenoxy,[30] dodecylmercapto[19] and other alkyl and aryl substituents,[31] which are not volatile in vacuum but soluble in organic solvents, were also been synthesized and studied. Ejsmont and R. Kubiak[20] determined diiodosubstituted tin phthalocyanine ($SnPcI_2$). The phthalocyanine ring is not strictly planar, and the complex crystalizes in a triclinic crystal system.

The ability to vary not only the substituents in the aromatic ring but also to introduce various axial substituents makes the chemistry of tin phthalocyanines richer than in the case of planar phthalocyanines. There are a lot of examples of tin(IV) phthalocyanine derivatives bearing complex alkyl and aryl substituents in axial positions,[21,31–33] which exhibit attractive photophysical and photochemical properties. Tin(IV) phthalocyanines are also capable of forming polymeric or oligomeric "face-to-face" structures through oxygen bridges,[34,35] which demonstrate non-linear optical properties. Konarev with co-authors[36,37] prepared a series of radical anion salts on the basis of Sn(II) and Sn(IV) derivatives and refined their crystal structures. Tin(IV) phthalocyanine are also promising to design coordination compounds with various ligands in axial positions, including metal-containing fragments.[38]

In recent decades, the chemistry of fluorinated complexes has begun to attract the attention of researchers again. This was due to the fact that the introduction of F-substituents into the phthalocyanine ring leads to an increase in sensitivity to analytical gases, a change in the type of conductivity.[39–41] Another important feature of fluoro-substituted ($MPcF_x$, x = 4, 8, 16) derivatives is the ability to transfer into the gas phase without decomposition in vacuum,[42,43] therefore, the method of physical vapour deposition (PVD) can be used to obtain films of these phthalocyanines. There is a number of works in the literature devoted both to the study of the structural properties of films of $MPcF_x$ (M = Co, Cu, Zn, VO) having planar structure and their application in various electronic devices.[44–47] At the same time, the structure of single crystals and thin films of phthalocyanines having a non-planar structure remain practically unexplored. The structure of $PbPcF_x$ (x = 4, 18) single crystals and their thin films as well as their chemiresistive sensor response to gaseous ammonia were studied in our previous work. Yutronkie with co-authors synthesized a SiF_2PcF_{16} derivative with two F-substituents in axial positions and that it is a stable n-type semiconductor with the mobility of charge carriers of 0.15 $cm^2 V^{-1} s^{-1}$.[48]

In this work, we demonstrate the structural diversity of fluorinated tin phthalocyanines depending on the synthesis technique. Tetrafluorinated phthalocyanine of tin(II) and tin(IV) were synthesized by two different techniques, namely by fusing fluorinated phthalonitriles with $SnCl_2$ and refluxing of the initial reagents in 1-chloronaphthalene, as a result of which their single crystals were grown and the crystal structure was determined. Thin films of Sn(II)PcF_4 deposited by vacuum sublimation were also investigated by X-ray diffraction and electron absorption spectroscopy methods.

Experimental

Synthetic pathway

To obtain halogenated tin phthalocyanines, two methods of synthesis were used: in the melt (Technique 1) and in the solution (Technique 2). Tin(II) chloride was used as a source of tin for the synthesis of all fluorinated phthalocyanine derivatives. 3-Fluorophthalonitrile (Fluorochem, cas: 65610-13-1, 95 %) and 4-fluorophthalonitrile (Sigma Aldrich, cas: 65610-14-2, 99 %) were used for the synthesis of tetrafluorosubstituted phthalocyanines with F-substituents in non-peripheral and peripheral positions (Figure 1).

Technique 1. $SnPcF_4$ were obtained by template synthesis from the corresponding fluorinated phthalonitriles with $SnCl_2$ (in a molar ratio 4:1) by fusion in an ampoule (T = 190–210 °C) during 4 h. The complexes were purified by double gradient sublimation in vacuum (T = 420–460 °C, P = 10^{-5} Torr). The synthesis and sublimation temperatures were chosen experimentally and depended on the phthalocyanine derivative.

Technique 2. Tin phthalocyanines were synthesized by refluxing the mixture of the initial reagents in 1-chloronaphthalene. For this purpose, a mixture of the corresponding fluorosubstituted phthalonitrile and $SnCl_2$ (in a mass ratio of 2:1) was boiled in 1-chloronaphthalene (10 mL) for 2 h. Then, the mixture was cooled, and the phthalocyanine was precipitated and washed with hexane, dried on a filter.

The yield of products after sublimation for both synthesis techniques averaged 40%.

$SnPcF_4$-p: $C_{32}H_{12}F_4N_8Sn$. Anal. Calc: C, 54.6; H, 1.7; N, 15.9; F, 10.8%. Found: C, 54.2; H, 1.5; N, 16.1; F, 11.1%. IR (KBr) ν cm^{-1}: 1614, 1596, 1479, 1396, 1331, 1256, 1221, 1163, 1111, 1072, 1043, 941, 914, 876, 862, 824, 770, 744, 731, 660, 644, 636, 588, 545, 522, 516, 505, 496. UV-Vis (THF) λ_{max} nm (lgε): 360 (4.41), 683 (4.67) (Figure S1a).

$SnCl_2PcF_4$-p: $C_{32}Cl_2H_{12}F_4N_8Sn$. Anal. Calc: C, 49.6; H, 1.6; N, 14.5; F, 9.8%. Found: C, 49.9 H, 1.5; N, 14.6; F, 10.1%. IR (KBr) ν cm^{-1}: 1614, 1587, 1481, 1443, 1394, 1342, 1315, 1258, 1223, 1161, 1113, 1078, 1043, 949, 899, 876, 826, 787, 768, 739, 723, 673, 646, 636, 594, 584, 577, 559, 548, 525, 515, 505, 490. UV-Vis (THF) λ_{max} nm (lgε): 363 (4.45), 703 (4.82) (Figure S1b).

$SnPcF_4$-np: $C_{32}H_{12}F_4N_8Sn$. Anal. Calc: C, 54.6; H, 1.7; N, 15.9; F, 10.8%. Found: C, 54.3; H, 1.5; N, 15.8; F, 11.0%. IR (KBr) ν cm^{-1}: 1616, 1589, 1508, 1487, 1456, 1394, 1333, 1248, 1221, 1167, 1115, 1071, 1042, 997, 924, 878, 800, 779, 750, 737, 669, 642, 600, 582, 563, 484. UV-Vis (THF) λ_{max} nm (lgε): 357 (4.44), 720 (4.76) (Figure S1a).

$SnCl_2PcF_4$-np: $C_{32}Cl_2H_{12}F_4N_8Sn$. Anal. Calc: C, 49.6; H, 1.6; N, 14.5; F, 9.8%. Found: C, 49.8 H, 1.6; N, 14.3; F, 9.6%. IR (KBr) ν cm^{-1}: 1618, 1587, 1489, 1465, 1396, 1335, 1249, 1234, 1221, 1167, 1117, 1077, 1043, 1001, 966, 957, 924, 897, 878, 837, 802, 777, 751, 737, 692, 669, 659, 642, 607, 591, 564, 517, 507. UV-Vis (THF) λ_{max} nm (lgε): 364 (4.50), 705 (4.89) (Figure S1b).

Thin films of $SnPc_4$ were deposited by a physical vapour deposition method using a vacuum universal station VUP-5M (Ukraine). The residual pressure was 10^{-5} Torr, the evaporation temperature was 460 °C, the substrate temperature was about 60 °C. The nominal thickness of the films was about 100 nm.

Methods

The elemental analysis was carried out using a Thermo Finnigan Flash 1112 Instrument (Center of collective use of NIIC SB RAS). Electronic absorption spectra of tin phthalocyanine solutions were recorded using a CF 2000 spectrophotometer (Russia). IR spectra of the complexes were measured on a Vertex 80 Bruker spectrometer in range from 100 to 600 cm^{-1} in polyethylene pellets and in the range from 600 to 4000 cm^{-1} in KBr pellets.

Single crystal XRD analysis of $SnPcF_4$ and $SnCl_2PcF_4$ crystals was performed using a Bruker D8 Venture single-crystal diffractometer (MoKα Incoatec IμS 3.0 microfocus X-ray source, 3-circle goniometer, PHOTON III CPAD detector). Data acquisition strategy consisted of several standard ϕ- and ω-scans with 0.5° frame width. Oxford Cryosystems Cryostream 800 plus open-flow nitrogen cooler was used to control the temperature of single-crystal samples during the experiment. APEX3 v.2019.1-0 software package[49] was used for indexing, raw data acquisition, data reduction and absorption correction. Obtained hklF datasets were processed in Olex2 v.1.5,[50] with SHELXT v.2018/2[51] used for the structure solution and SHELXL v.2018/3[52] used for the refinement. All non-hydrogen atoms were refined anisotropically. Hydrogen atoms were located geometrically and refined using the riding model. The resulting CIF files was deposited to the Cambridge Crystallographic Data Center (CCDC) (No. 2310956-2310960) and can be obtained free of charge at *www.ccdc.cam.ac.uk/structures*.

XRD analysis of bulk powders and thin films of tin phthalocyanines was performed at room temperature using a Bruker D8 Advance powder diffractometer (Bragg-Brentano geometry with vertical θ-θ goniometer, CuKα sealed X-ray tube, LYNXEYE XE-T compound silicon strip detector, 0.01° scan step). Hirshfeld surface analysis was carried out in CrystalExplorer 21.5.[53]

Thermogravimetric (TG) analysis of phthalocyanines was carried out in argon atmosphere at a heating rate of 10 C min^{-1} using TG 209 F1 Iris Thermo Microbalance (NETZSCH).

Mass spectra and exact masses for the compounds were obtained using Thermo Scientific Double Focusing System (DFS) high resolution mass-spectrometer. Samples weighing about 2 mg were injected into the mass spectrometer by direct injection. The mass spectrometer used electron ionization with 70 eV ionization energy. Measurements of the exact masses of the ions were performed with respect to the standard lines of perfluorokerosene (PFK).

Results and Discussion

Synthesis of tetrafluorosubstituted tin phthalocyanines

In the case of tetrafluorosubstituted phthalocyanines, F-substituents can be located in peripheral (p) and non-peripheral (np) positions of the benzene rings (Figure 1). For their synthesis, 4-fluorophthalonitrile and 3-fluorophthalonitrile were used as initial reagents, respectively.

Tetrafluorosubstituted phthalocyanines of tin were synthesized by two techniques: by fusion of the corresponding phthalonitrile derivative with $SnCl_2$ (Technique 1) and by refluxing of the initial reagents in 1-chloronaphthalene (Technique 2) as shown in Scheme 1.

The blue solids obtained by Technique 1 were sublimed in vacuum (10^{-5} Torr). As a result of the sublimation, single crystals of $SnPcF_4$-p and $SnPcF_4$-np were isolated from the sublimate. In addition to the elemental analysis, the composition of the complexes was confirmed by mass spectrometry data (Figure S2). The most intense peaks *m/z*=704.014 in the mass-spectra of both compounds

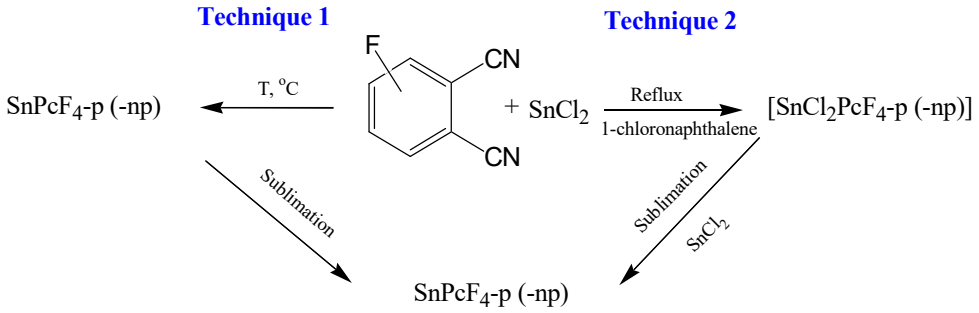

Scheme 1. Synthetic pathways of tetrafluorosubstituted tin phthalocyanines.

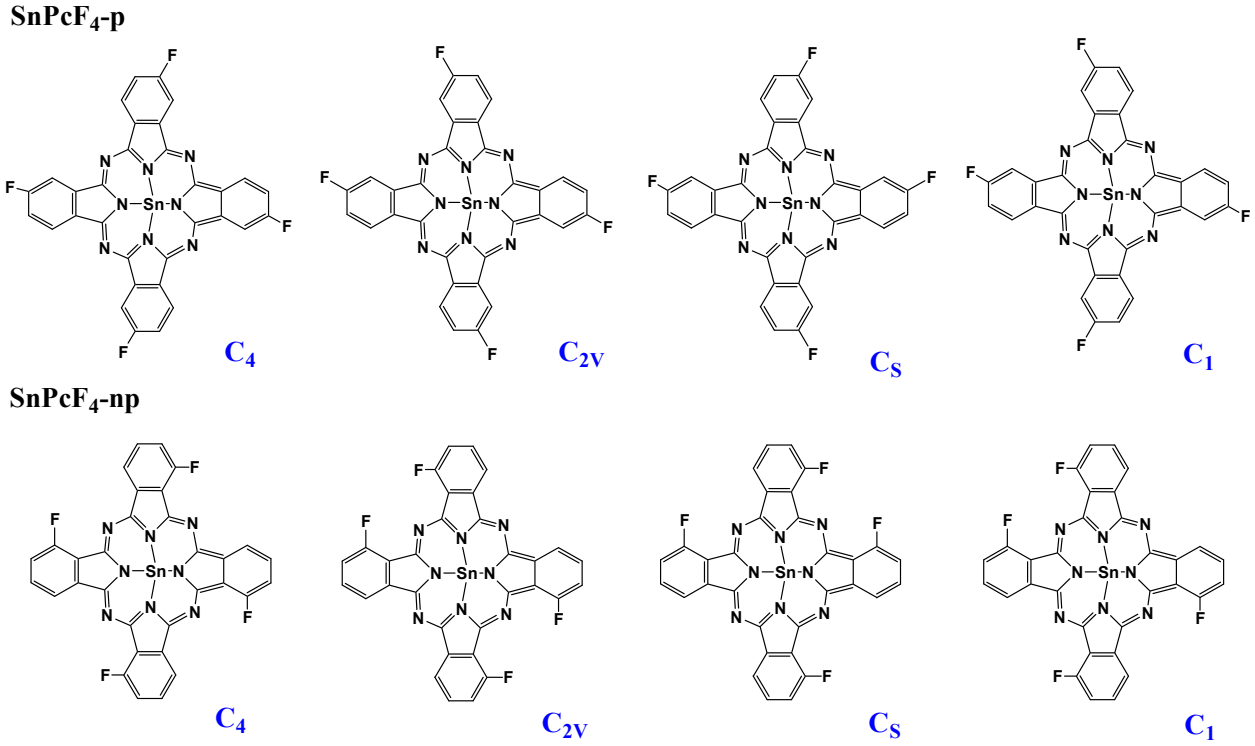

Figure 1. Isomers of tetrafluorosubstituted tin(II) phthalocyanines with F-substituents in peripheral (p) and non-peripheral (np) positions.

correspond to the molecular ions $(SnPcF_4)^+$·(calc. *m/z*=704.014, $(C_{32}H_{12}N_8F_4{}^{120}Sn)^+$). At the same time, as a result of the synthesis in solution (Technique 2), tin(IV) complexes, namely $SnCl_2PcF_4$-p and $SnCl_2PcF_4$-np, were formed instead of tin(II) complexes.

Usually when synthesized by the methods of tetramerization of monosubstituted phthalonitriles, tetrasubstituted phthalocyanines are formed as a mixture of four regioisomers (Figure 1).

According to the literature data,[54] separation of the isomers is very difficult and possible only for highly soluble phthalocyanines with bulky alkyl substituents, which do not aggregate in solutions. High-performance liquid chromatography and medium-pressure liquid chromatography utilizing special modified silica gels are used for their separation, while the method of ^{1}H NMR and ^{13}C NMR are used for the determination of the ratio of isomers in solutions.[55,56] It was shown that the ratio of isomers depends on the type of substituents and central metals as well as on the synthetic procedure.[57,58] Usually all four regioisomers are present in the mixture[57,58] with a maximal contribution of the lowest symmetric one. Fluorinated tin phthalocyanines have very poor solubility in conventional organic solvents and even when dissolved in tetrahydrofuran and quinoline, their concentration is only about 10^{-6} M. This makes it impossible to separate isomers by chromatographic methods. It was also not possible to separate $SnPcF_4$ isomers during their sublimation in vacuum. Therefore, the presence of all four isomers in the mixture can only be judged by indirect data. For example, Nizovtsev[59] demonstrated that the experimental IR spectrum of np-$ZnPcF_4$ coincided well with the calculated spectrum obtained as the sum of the spectra of four isomers in the ratio equal to the Boltzmann′s factors calculated for the synthesis temperature of the studied compounds.

Optical absorption spectra of $SnPcF_4$ and $SnCl_2PcF_4$ derivatives are shown in Figure S1. Similarly to other phthalocyanines, spectra of $SnPcF_4$ and $SnCl_2PcF_4$ solutions are characterized by two bands: the Q-band attributed to the electron transitions from HOMO a_{1u} to the LUMO e_g and the B-band due to the transitions from the HOMO a_{2u} to the LUMO e_g in visible and ultraviolet spectral regions, respectively.[60] The introduction of F-substituents to non-peripheral positions of phthalocyanine ring leads to the bathochromic shift of the Q-band in comparison with the complexes bearing the substituents in peripheral positions, *e.g.* from 683 to 720 nm for $SnPcF_4$ derivatives and from 703 to 705 nm for $SnCl_2PcF_4$ derivatives. Similar shifts of the Q-band maxima were also observed for other $MPcF_4$-np (M=Co, Cu, Fe, Pd, Pb, VO) complexes compared to $MPcF_4$-p ones, which ranged from 6 to 47 nm depending on the central metals.[61]

XRD study of $SnPcF_4$-p and $SnPcF_4$-np complexes

$SnPcF_4$-p and $SnPcF_4$-np complexes form polycrystalline powders with a dull dark blue colour after sublimation. The data of their TG analysis in argon atmosphere are shown in Figure S3. Both complexes start to sublime with partial decomposition at the temperature above 300 °C.

$SnPcF_4$-p crystals have the shape of thick rectangular plates. The molecular structure and packing diagrams of $SnPcF_4$-p are shown in Figure 2.

$SnPcF_4$-p crystallizes in the triclinic P-1 space group with Z=2, Z'=1 and one symmetrically independent molecule in the unit cell. The unit cell parameters and refinement details are given in Table 1. A $SnPcF_4$-p molecule has the shape of a "shuttlecock" (Figure 2a) with a Sn atom displaced from the central plane of the macrocycle by 1.115 Å due to the presence of the lone electron pair. The

Sn-N bond lengths vary in the range of 2.253(2)–2.261(2) Å (2.258 Å mean). Each of the four fluorine atoms is disordered in two positions, with occupancy ratios ranging from 0.605/0.395 to 0.554/0.446. As can be seen from Figure 2b, $SnPcF_4$-p molecules pack perpendicularly to the b-axis and form isolated layers along the a-axis, while intermolecular contacts along c-axis limited mainly by F…F and F…H interactions between terminal atoms.

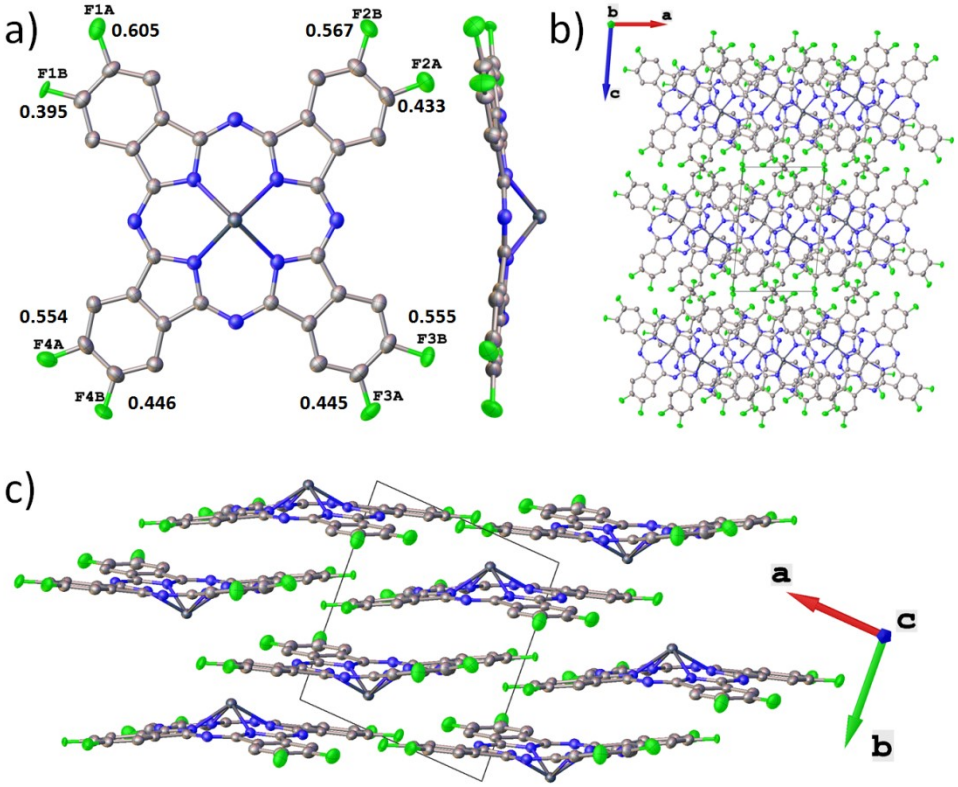

Figure 2. Molecular structure (a), packing along the b axis (b) and packing along the c axis (c) of $SnPcF_4$-p.

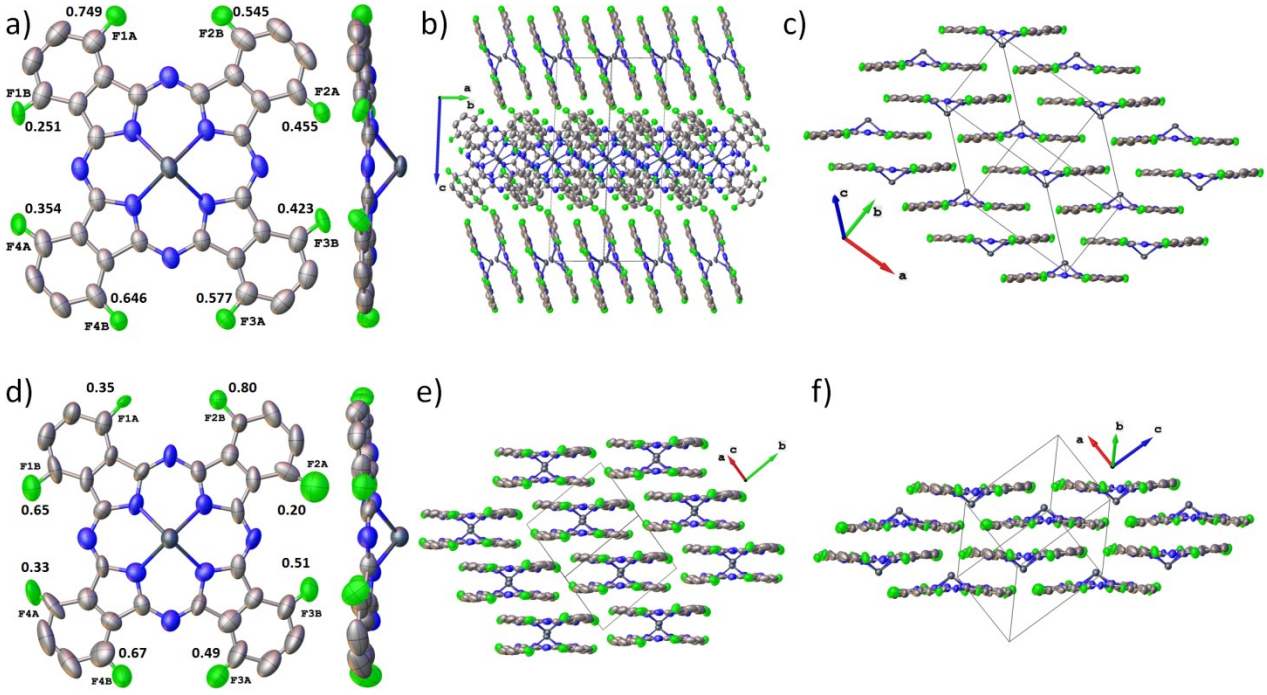

Figure 3. Molecular structure (a) and packing (b,c) for the monoclinic polymorph of $SnPcF_4$-np and molecular structure (d) and packing (e,f) for the triclinic polymorph of $SnPcF_4$-np.

Table 1. Unit cell parameters and refinement details for $SnPcF_4$-p and $SnPcF_4$-np crystal structures.

Compound	$SnPcF_4$-p	$SnPcF_4$-np (m)	$SnPcF_4$-np (t)
Empirical formula	$C_{32}H_{12}F_4N_8Sn$	$C_{32}H_{12}F_4N_8Sn$	$C_{32}H_{12}F_4N_8Sn$
Formula weight	703.19	703.19	703.19
Temperature, K	150.00	150	150
Crystal system	triclinic	monoclinic	triclinic
Space group	P-1	P21/c	P-1
a, Å	8.9474(2)	11.6812(2)	8.853(2)
b, Å	10.4272(3)	8.47710(10)	11.505(3)
c, Å	13.6656(4)	25.4297(5)	12.683(3)
α, °	96.3420(10)	90	89.732(6)
β, °	94.0000(10)	93.9290(10)	80.890(6)
γ, °	94.2790(10)	90	85.009(6)
Volume, $Å^3$	1259.70(6)	2512.20(7)	1270.7(6)
Z	2	4	2
ρ_{calc}, g/cm^3	1.854	1.859	1.838
μ, mm^{-1}	1.087	1.090	1.078
F(000)	692.0	1384.0	692.0
Crystal size, mm^3	0.12 × 0.08 × 0.04	0.08 × 0.06 × 0.03	0.08 × 0.025 × 0.025
Radiation	MoKα (λ = 0.71073)	MoKα (λ = 0.71073)	MoKα (λ = 0.71073)
2Θ range for data collection, °	3.944 to 61.08	4.582 to 61.048	3.554 to 41.726
Index ranges	-11 ≤ h ≤ 12, -14 ≤ k ≤ 14, -19 ≤ l ≤ 19	-16 ≤ h ≤ 16, -9 ≤ k ≤ 12, -36 ≤ l ≤ 35	-8 ≤ h ≤ 8, -11 ≤ k ≤ 11, -12 ≤ l ≤ 12
Reflections collected	24867	42726	9601
Independent reflections	7695 [R_{int} = 0.0349, R_{sigma} = 0.0427]	7668 [Rint = 0.0349, Rsigma = 0.0294]	2673 [Rint = 0.1464, Rsigma = 0.1281]
Data/restraints/parameters	7695/0/446	7668/1/446	2673/37/446
Goodness-of-fit on F^2	1.059	1.025	1.006
Final R indexes [I>=2σ (I)]	R1 = 0.0383, wR2 = 0.0901	R1 = 0.0344, wR2 = 0.0793	R1 = 0.0748, wR2 = 0.1651
Final R indexes [all data]	R1 = 0.0522, wR2 = 0.0980	R1 = 0.0545, wR2 = 0.0888	R1 = 0.1330, wR2 = 0.1954
Largest diff. peak/hole, e $Å^{-3}$	1.68/-0.89	1.22/-0.90	1.50/-0.46
CCDC deposition No.	2310956	2310957	2310958

The structure of one such layer is shown in Figure 2c. Each $SnPcF_4$-p molecule is adjacent to four molecules with partially overlapping aromatic rings forming a network of π-π interactions within the molecular layer. The average distance between neighboring molecules is 3.35 Å. The same packing style was previously observed in $VOPcF_8$ crystals.[62] The unit cell parameters of $SnPcF_4$-p are also very similar to $VOPcF_8$ and the crystal structures of these two compounds can be considered isomorphous.

Two crystalline phases were isolated from the $SnPcF_4$-np powder obtained by sublimation: the monoclinic phase (Z = 4, Z' = 1), which grew in the form of large plates of dark blue colour with a metallic luster, and the triclinic phase (Z = 2, Z' = 1), which grew in the form of small thin plates of the same colour. The molecular structure and packing diagrams for both $SnPcF_4$-np phases are shown in Figure 3. $SnPcF_4$-np molecules have the same "shuttlecock" shape as $SnPcF_4$-p but with fluorine atoms located in non-peripheral positions. The Sn(II) atom is displaced from the macrocycle plane by 1.126 Å in the monoclinic polymorph and by 1.136 Å in the triclinic polymorph with Sn-N bond lengths of 2.257–2.272 Å (2.265 Å mean) and 2.253–2.286 Å (2.275 Å mean), respectively. The occupancy rates of fluorine atoms in $SnPcF_4$-np crystal structures deviate more strongly from the ratio of 0.5/0.5 than in $SnPcF_4$-p (Figure 3a,d), indicating that substituents in non-peripheral positions may have a greater influence on the molecular packing and that not all positions are favourable for fluorine atoms. $SnPcF_4$-np molecules in the monoclinic polymorph are arranged in isolated layers perpendicular to the c-axis (Figure 3b).

The molecules in the adjacent layers are rotated relative to each other by 79.96°. The structure of the molecular layer differs from $SnPcF_4$-p, since each molecule contacts (and participates in π-π interactions) with three other molecules instead of four (Figure 3c), and the molecules along the same line are oriented in the same direction (either "up" or "down") instead of alternating "up" and "down" configurations in $SnPcF_4$-p. The distances between the molecule and its three neighbours are 3.371 Å, 3.299 Å and 3.197 Å. $SnPcF_4$-np molecules in the triclinic polymorph are packed into molecular chains (Figure 3e). When viewed from the side (Figure 3f), it becomes clear that the mutual arrangement of molecules in the triclinic polymorph is very similar to the monoclinic one, but since the individual molecular chains are displaced relative to each other, this packing style can no longer be called "layered". The distances between molecules in one chain are 3.291 and 3.347 Å.

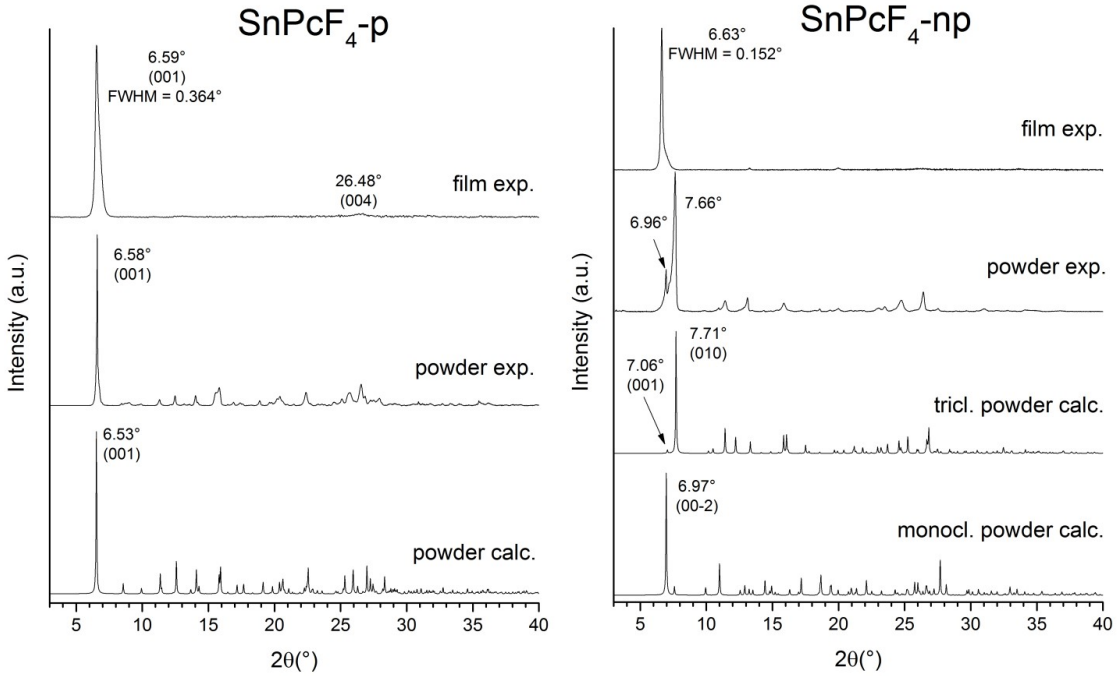

Figure 4. XRD patterns for $SnPcF_4$-p and $SnPcF_4$-np powders and films in comparison with the XRD patterns calculated from the single crystal data.

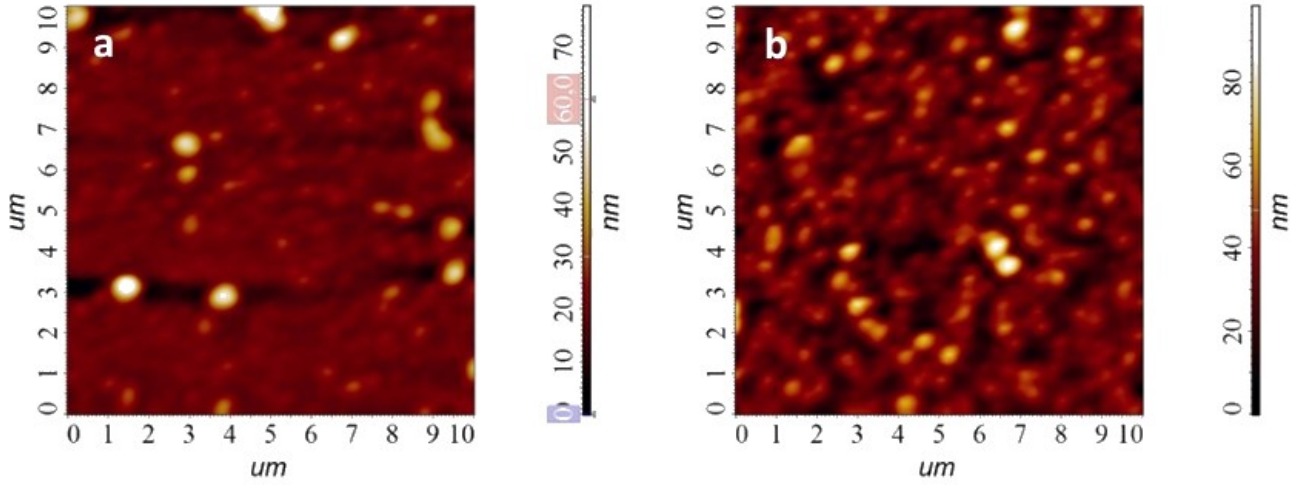

Figure 5. AFM images of the surfaces of the $SnPcF_4$-p (a) and $SnPcF_4$-np (b) films.

XRD patterns for $SnPcF_4$-p and $SnPcF_4$-np powders and thin films are shown in Figure 4 compared to powder patterns calculated from single crystal data. The experimental powder pattern of $SnPcF_4$-p coincides well with the calculated one with the exception of three weak diffraction peaks at 8.73°, 9.02°, and 9.67° 2θ, indicating the presence of another minor phase. It should be noted that the experimental data of the elemental analysis and the mass spectrum are in good agreement with the calculated ones, for this reason, this secondary phase is most likely another polymorphic modification and not a phase with a different chemical composition. XRD pattern of $SnPcF_4$-p thin film features one strong peak, which indicates the presence of strong preferred orientation of $SnPcF_4$-p crystallites relative to the substrate surface. 2θ position of this peak (6.59°) matches well with (001) peak on powder diffraction pattern, so $SnPcF_4$-p thin film most likely consists of the same crystal phase as bulk powder. Since we know the crystal structure $SnPcF_4$-p and the direction of preferred orientation in the thin film, it is possible to calculate the angle between $SnPcF_4$-p molecules (mean squares plane through all atoms except tin and hydrogen) and the substrate surface, which turned out to be equal to 89.24°.

The XRD pattern of the $SnPcF_4$-np powder has one strong diffraction peak at 7.66° 2θ, which corresponds to the plane (010) of the triclinic phase, and one less intense peak at 6.96° 2θ, corresponding to the peak (00-2) of the monoclinic phase. This means that the bulk $SnPcF_4$-np

powder contains both polymorph phases in comparable amounts. Similarly to the $SnPcF_4$-p, the XRD pattern of a $SnPcF_4$-np film also contains one strong diffraction peak, but its 2θ position does not coincide with any peaks from either monoclinic or triclinic $SnPcF_4$-np phases. Because of this, we cannot draw any clear conclusions about the orientation of $SnPcF_4$-np molecules relative to the substrate surface, even though the $SnPcF_4$-np film definitely has strong preferred orientation. It should also be noted that the diffraction peak on the XRD pattern of a $SnPcF_4$-np film has a noticeable asymmetry on the right side, which indicates the presence of a second diffraction peak that is not resolved against the background of the stronger first peak. The approximate 2θ position of this second peak coincides with either (00-2) peak of the monoclinic phase or (001) peak of the triclinic phase, which means that the $SnPcF_4$-np film may contain at least two crystal phases. Using the Scherrer equation, it is possible to estimate the size of coherent scattering region for both $SnPcF_4$-p and $SnPcF_4$-np films using the FWHM values of observed diffraction peaks. Taking into account the instrumental peak broadening of 0.05°, the Scherrer equation gives values of 25 nm for $SnPcF_4$-p and 75 nm for $SnPcF_4$-np, which shows that $SnPcF_4$-np film has significantly better crystallinity compared to the $SnPcF_4$-p one.

The method of atomic force microscopy was used to study the morphology of the films. Figure 5 shows AFM images of the surface of $SnPcF_4$-p and $SnPcF_4$-np films. The surface of $SnPcF_4$-p films is formed by slightly elongated blurred aggregates; the RMS roughness value is 6.7 nm. $SnPcF_4$-np films are formed by clearly visible rounded aggregates with an average size of about 200 nm, RMS is 2.4 nm.

XRD study of $SnCl_2PcF_4$-p and $SnCl_2PcF_4$-np complexes

Single crystals of $SnCl_2PcF_4$-p and $SnCl_2PcF_4$-np were selected from the product obtained by Technique 2 in 1-chloronaphthalene. The XRD analysis showed that the formed crystals consisted of Sn(IV) phthalocyanine molecules with two chlorine atoms coordinated with the Sn atom in axial positions. The formation of $SnCl_2PcF_4$-p and $SnCl_2PcF_4$-np was also confirmed by the data of elemental analysis and IR spectroscopy. IR spectra of $SnCl_2PcF_4$-p are compared with that of $SnPcF_4$-p in Figure 6. A group of bands in the range from 1400 to 1700 cm^{-1}, which correspond to C=C and C=N stretching vibrations. The bands corresponding to ν(C=C) have almost the same positions in the spectra of both $SnCl_2PcF_4$-p and $SnPcF_4$-p. The most pronounced shift and intensity change of the bands in the spectra of $SnCl_2PcF_4$-p is observed at about 740 cm^{-1} and in the range of 820–900 cm^{-1}.

According to the previous DFT spectra calculations,[63] these bands mostly can be attributed to the C_α-N_α-C_α and C_α-N_β-C_α deformations with the involvement of Sn-N_α stretching vibrations. The band at 744 cm^{-1} in the $SnPcF_4$-p spectrum shift to 739 cm^{-1} in the case of $SnCl_2PcF_4$-p and also new bands at 620 and 843 cm^{-1} appear in the spectrum of $SnCl_2PcF_4$-p. The bands corresponding to δ(C_β-C_α-N_β), δ(C_α-N_β-C_α) and ν(C_α-N_α) at 1072 and 1332 cm^{-1} in the IR spectrum of $SnPcF_4$-p shifts to 1084 and 1343 cm^{-1} in the case of $SnCl_2PcF_4$-p, respectively. The most remarkable shift is also observed in the far IR region. The new peaks at 327 and 337 cm^{-1} appear in the spectrum of $SnCl_2PcF_4$-p, which can be attributed to Sn-Cl stretching vibrations in combination with the pyrrole ring out-of-plane bending.[64]

$SnCl_2PcF_4$-p crystallizes in the P-1 space group with Z=1 and Z'=0.5. The unit cell parameters and details of the structure refinement are given in Table 2. The $SnCl_2PcF_4$-p molecule is centrosymmetric and contains two types of halogen substituents: two axial chlorine atoms coordinated to the central Sn(IV) atom with a Sn-Cl bond length of 2.431(1)Å and four peripheral fluorine atoms, each of which is disordered in two positions with a ratio of 0.378/0.622 or 0.502/0.498 (Figure 7). Since the $SnCl_2PcF_4$-p molecule is centrosymmetric, the Sn atom lies exactly in the macrocycle plane with Sn-N bond lengths of 2.056(2) Å and 2.050(3) Å. The angle between the normal to the macrocycle plane and the Sn-Cl bond is 0.27°, and the N-Sn-N angles deviate from 90° only by 0.49°, which gives the octahedral coordination of the Sn(IV) atom. $SnCl_2PcF_4$-p packs in isolated layers perpendicular to the c-axis (Figure 7b). Inside one such layer, the molecules are arranged in such a way that the gap between two neighboring molecules in one row is occupied by axial Cl atoms from one molecule from the row above and one molecule from the row below (Figure 7c). The distance between these Cl atoms is 3.738 Å, while the distance between molecular planes in adjacent rows is 3.344 Å.

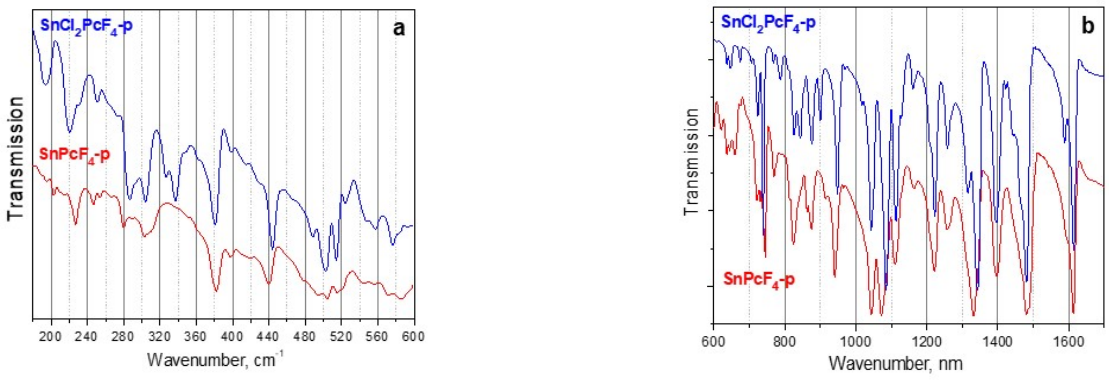

Figure 6. FT-IR spectra of $SnCl_2PcF_4$-p and $SnPcF_4$-p in the far IR region (**a**, in polyethylene pellets) and middle IR region (**b**, in KBr pellets).

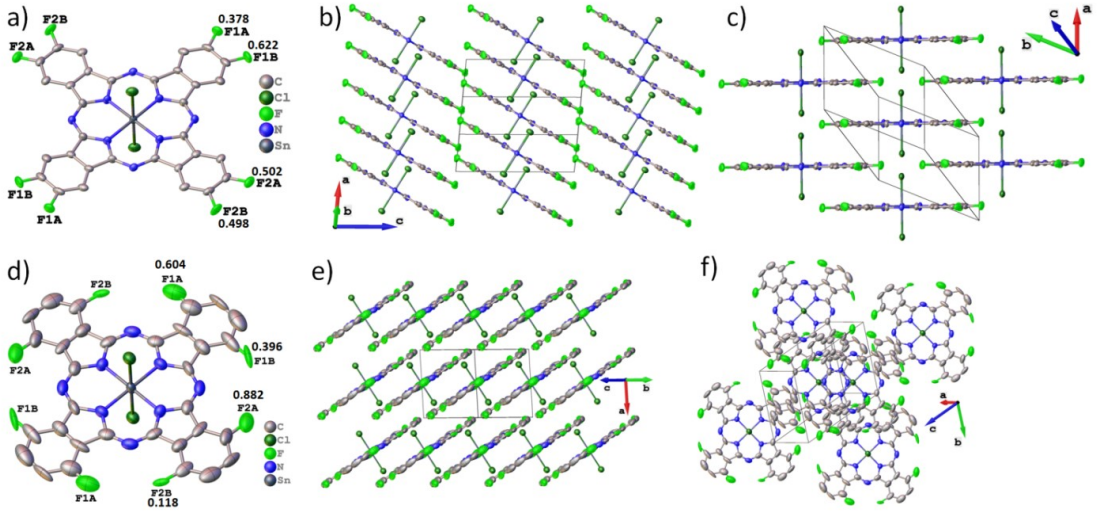

Figure 7. Molecular structure (a) and packing diagrams (b,c) for $SnCl_2PcF_4$-p and molecular structure (d) and packing diagrams (e,f) for $SnCl_2PcF_4$-np.

Table 2. Unit cell parameters and structure refinement details for $SnCl_2PcF_4$-p and $SnCl_2PcF_4$-np.

Compound	$SnCl_2PcF_4$-p	$SnCl_2PcF_4$-np
Empirical formula	$C_{32}H_{12}Cl_2F_4N_8Sn$	$C_{32}H_{12}Cl_2F_4N_8Sn$
Formula weight	774.09	774.09
Temperature, K	150	150
Crystal system	triclinic	triclinic
Space group	P-1	P-1
a, Å	7.3598(4)	7.6034(11)
b, Å	8.8157(5)	9.0559(14)
c, Å	12.3576(7)	10.6495(14)
α, °	69.508(2)	75.667(4)
β, °	85.438(2)	82.964(4)
γ, °	65.814(2)	80.267(4)
Volume, $Å^3$	683.20(7)	697.73(17)
Z	1	1
ρ_{calc}, g/cm^3	1.881	1.842
μ, mm^{-1}	1.201	1.176
F(000)	380.0	380.0
Crystal size, mm^3	0.1 × 0.08 × 0.01	0.06 × 0.04 × 0.015
Radiation	MoKα (λ = 0.71073)	MoKα (λ = 0.71073)
2Θ range for data collection, °	5.324 to 59.08	3.962 to 51.298
Index ranges	$-10 \le h \le 10$, $-12 \le k \le 11$, $-17 \le l \le 17$	$-8 \le h \le 9$, $-11 \le k \le 11$, $-12 \le l \le 12$
Reflections collected	8735	7121
Independent reflections	3783 [R_{int} = 0.0496, R_{sigma} = 0.0808]	2626 [R_{int} = 0.0705, R_{sigma} = 0.0990]
Data/restraints/parameters	3783/0/234	2626/18/234
Goodness-of-fit on F^2	1.022	1.041
Final R indexes [I>=2σ (I)]	R_1 = 0.0485, wR_2 = 0.0856	R_1 = 0.0598, wR_2 = 0.1277
Final R indexes [all data]	R_1 = 0.0688, wR_2 = 0.0943	R_1 = 0.0934, wR_2 = 0.1406
Largest diff. peak/hole, e $Å^{-3}$	1.11/-0.75	0.96/-0.91
CCDC deposition No.	2310959	2310960

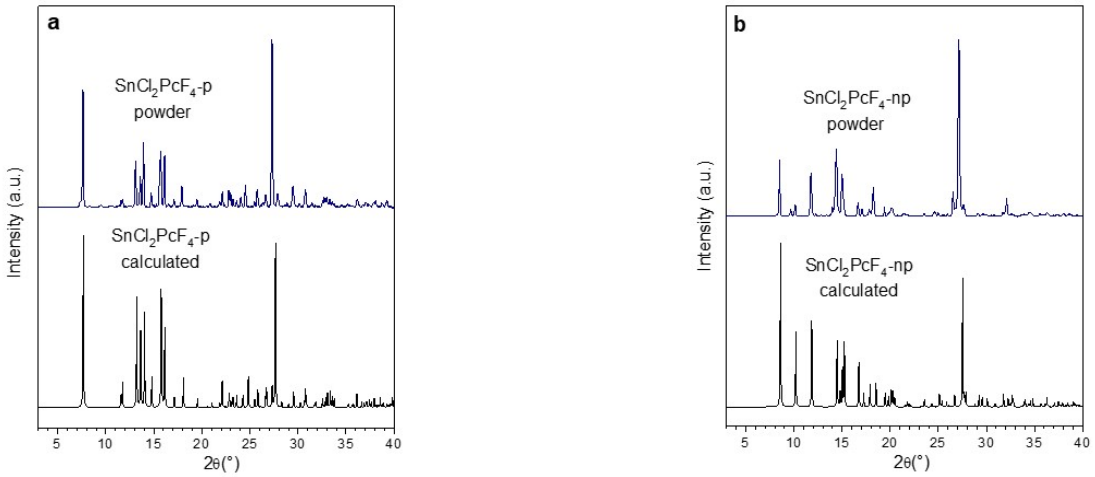

Figure 8. XRD patterns for $SnCl_2PcF_4$-p (a) and $SnCl_2PcF_4$-np (b) powders in comparison with the XRD patterns calculated from the single crystal data.

$SnCl_2PcF_4$-np also crystallizes in the P-1 space group with Z'=0.5 and contains two axial chlorine atoms coordinated to a central Sn(IV) atom with a Sn-Cl bond length of 2.436(2) Å and four peripheral fluorine atoms disordered in two positions with the ratios of 0.604/0.396 or 0.882/0.118 (Figure 7d). The angle between the normal to the macrocycle plane and the Sn-Cl bond is 0.52°. The Sn-N bond lengths are 2.038(5) Å and 2.047(5) Å and the N-Sn-N angles are almost equal to 90° (89.99°/90.01°). $SnCl_2PcF_4$-np molecules are packed into 2D layers (Figure 7e) with the molecules arranged in such a way that the gap between four molecules in one layer is occupied by two axial Cl atoms from the molecules in the adjacent layers. The distance between these Cl atoms is 4.343 Å, and average distance between the molecular planes in adjacent rows is 3.201 Å. Thus, both $SnCl_2PcF_4$-p and $SnCl_2PcF_4$-np molecules have identical Sn(IV) coordination despite different positions of fluorine atoms and packing style.

Figure 8 shows powder diffraction patterns of $SnCl_2PcF_4$-p and $SnCl_2PcF_4$-np directly after synthesis compared to the powder patterns calculated from the crystal structures of Sn(II) and Sn(IV) tetrafluorinated phthalocyanines described above. The main peaks on the XRD patterns of both $SnCl_2PcF_4$-p and $SnCl_2PcF_4$-np bulk powders coincide well with the calculated ones from the single-crystal data. There are also low-intensity peaks that do not correspond to either phthalocyanine Sn(II) or Sn(IV) on the diffractograms. For $SnCl_2PcF_4$-p these peaks are located at 7.32°, 8.32°, 9.50°, 10.39°, 10.69°, and 16.54° 2θ, and for $SnCl_2PcF_4$-np – at 9.67°, 11.26°, 12.29°, 12.82° and 13.40° 2θ. It is necessary to pay attention to our following observations. Sublimation of $SnCl_2PcF_4$-p and $SnCl_2PcF_4$-np powders obtained as a result of Technique 2 leads to the formation of $SnPcF_4$-p and $SnPcF_4$-np. The XRD patterns of $SnCl_2PcF_4$-p and $SnCl_2PcF_4$-np powders after their sublimation in the presence of $SnCl_2$ are shown in Figure S4. In our opinion, the formation of $SnPcF_4$ may occur due to the residual content of $SnCl_2$ after the synthesis, which can act as a reducing agent and lead to the reduction of $Sn(IV)Cl_2PcF_4$ to $Sn(II)PcF_4$. A similar process was described earlier for unsubstituted tin phthalocyanines.[65]

Conclusions

In this work, tetrafluorinated phthalocyanines of tin were synthesized by two different techniques, namely by fusing fluorinated phthalonitriles with $SnCl_2$ (Technique 1) and refluxing of the initial reagents in 1-chloronaphthalene (Technique 2), as a result of which their single crystals were grown, and the crystal structure was determined. It was found that the synthesis method affected the composition and structure of the obtained complexes. It was shown that during the synthesis by Technique 1, $Sn(II)PcF_4$ complexes were formed. At the same time, during the synthesis by Technique 2, Sn(IV) complexes were formed, namely $SnCl_2PcF_4$. $SnPcF_4$-p crystallizes in the triclinic P-1 space group. Two crystalline phases were isolated from the $SnPcF_4$-np powder obtained by sublimation: the monoclinic phase and the triclinic. $SnPcF_4$ molecules have a "shuttlecock" shape and a layered packing motif. The XRD analysis of $SnCl_2PcF_4$-p and $SnCl_2PcF_4$-np showed that they crystals consisted of Sn(IV) phthalocyanine molecules with two chlorine atoms coordinated with the Sn atom in axial positions. The formation of $SnCl_2PcF_4$-p and $SnCl_2PcF_4$-np was also confirmed by the data of elemental analysis and IR spectroscopy. Sn(IV) complexes have a layered packing motifs but with adjacent layers more distant from each other due to the presence of Cl-atoms in axial positions. Thin films of $Sn(II)PcF_4$ complexes were obtained by physical vapor deposition method. The XRD pattern of a $SnPcF_4$-p film has one strong peak, which indicates a strong preferred orientation of $SnPcF_4$-p crystallites relative to the substrate surface. Similarly to $SnPcF_4$-p, the XRD pattern of a $SnPcF_4$-np film contains one strong diffraction peak, but its 2θ position does not coincide with any peaks from either monoclinic or triclinic $SnPcF_4$-np phases.

Acknowledgements. The study was funded by the Russian Science Foundation [grant number 22-73-00145]. The authors also acknowledge the Ministry of Science and Higher Education of the Russian Federation for access to the centres of collective use and the Multi-Access Chemical Research Center SB RAS for mass spectra and exact masses measurements.

References

1. Yalazan H., Ömeroğlu İ., Çelik G., Kantekin H., Durmuş M. *Inorg. Chim. Acta* **2023**, *551*, 121480.
2. El-Damhogi D.G., ELesh E., Ibrahim A.H., Mosaad S., Makhlouf M.M., Mohamed Z. *Radiat. Phys. Chem.* **2022**, *195*, 110060.
3. Moiseeva E. O., Trashin S., Korostei Y.S., Ullah Khan S., Kosov A.D., De Wael K., Dubinina T.V., Tomilova L.G. *Polyhedron* **2021**, *200*, 115136.
4. Ohta H., Kambayashi T., Nomura K., Hirano M., Ishikawa K., Takezoe H., Hosono H. *Adv. Mater.* **2004**, *16*, 312.
5. Zhang X., Gao N., Li Y., Xie L., Yu X., Lu X., Gao X., Gao J., Shui L., Wu S., Liu J.-M. *ACS Appl. Energy Mater.* **2020**, *3*, 7832.
6. Cranston R.R., Vebber M.C., Rice N.A., Tonnelé C., Castet F., Muccioli L., Brusso J.L., Lessard B.H. *ACS Appl. Electron. Mater.* **2021**, *3*, 1873.
7. Grant T.M., Rice N.A., Muccioli L., Castet F., Lessard B.H. *ACS Appl. Electron. Mater.* **2019**, *1*, 494.
8. Acharjya S., Chen J., Zhu M., Peng C. *Greenhouse Gases Sci. Technol.* **2021**, *11*, 1191.
9. Du C., Yu J., Huang J., Jiang Y. *Energ. Proced.* **2011**, *12*, 519.
10. El-Nahass M.M., Farid A.M., Abd El-Rahman K.F., Ali H.A.M. *Phys. B Condens. Matter* **2008**, *403*, 2331.
11. Friedel M.K., Hoskins B.F., Martin R.L., Mason S.A. *J. Chem. Soc. D* **1970**, 400.
12. Kubiak R., Janczak J. *J. Alloys Compd.* **1992**, *189*, 107.
13. Bodek L., Cebrat A., Piatkowski P., Such B. *J. Phys. Chem. C* **2019**, *123*, 9209.
14. Lu S., Huang M., Huang G., Guo Q., Li H., Deng J., Zhang C., Yu Y. *Nanoscale Adv.* **2022**, *4*, 1213.
15. Roy M.S., Deol Y.S., Janu Y., Gautam A.K., Kumar M., Balraju P., Sharma G.D. *J. Mater. Sci. Mater. Electron.* **2009**, *20*, 984.
16. Khene S., Ogunsipe A., Antunes E., Nyokong T. *J. Porphyrins Phthalocyanines* **2007**, *11*, 109.
17. Odabaş Z., Altindal A., Bulut M. *Synth. Met.* **2011**, *161*, 1742.
18. Pişkin M., Öztürk Ö.F., Odabaş Z. *Karaelmas Fen ve Mühendislik Derg.* **2017**, *7*, 627.
19. Khene S., Geraldo D.A., Togo C.A., Limson J., Nyokong T. *Electrochim. Acta* **2008**, *54*, 183.
20. Ejsmont K., Kubiak R. *Acta Crystallogr. Sect. C Cryst. Struct. Commun.* **1997**, *53*, 1051.
21. Beltrán H.I., Esquivel R., Lozada-Cassou M., Dominguez-Aguilar M A., Sosa-Sánchez A., Sosa-Sánchez J L., Höpfl H., Barba V., Luna-García R., Farfán N., Zamudio-Rivera L S. *Chem. Eur. J.* **2005**, *11*, 2705.
22. Bodek L., Engelund M., Cebrat A., Such B. *Beilstein J. Nanotechnol.* **2020**, *11*, 821.
23. El-Nahass M.M., Abd-El-Rahman K.F., Al-Ghamdi A.A., Asiri A.M. *Phys. B Condens. Matter* **2004**, *344*, 398.
24. Rogers D., Osborn M.R.S. *Chem. Commun.* **1971**, 840.
25. El-Nahass M.M., Yaghmour S. *Appl. Surf. Sci.* **2008**, *255*, 1631.
26. Obaidulla S.M., Giri P.K., *Appl. Phys. Lett.* **2015**, *107*.
27. Obaidulla SK.Md., Goswami D.K., Giri P.K. *Appl. Phys. Lett.* **2014**, *104*, 213302.
28. Obaidulla S.M., Giri P.K. *J. Mater. Chem. C* **2015**, *3*, 7118.
29. Louzada M., Britton J., Nyokong T., Khene S. *J. Phys. Chem. A* **2017**, *121*, 7165.
30. Pişkin M., Can N., Odabaş Z., Altlndal A. *J. Porphyrins Phthalocyanines* **2018**, *22*, 189.
31. Maree S., Phillips D., Nyokong T. *J. Porphyrins Phthalocyanines* **2002**, *6*, 17.
32. Melville O.A., Grant T.M., Lochhead K., King B., Ambrose R., Rice N.A., Boileau N.T., Peltekoff A.J., Tousignant M., Hill I.G., Lessard B.H. *ACS Appl. Electron. Mater.* **2020**, *2*, 1313.
33. Slodeka A., Schnurpfeil G., Wöhrle D. *J. Porphyrins Phthalocyanines* **2017**, *21*, 811.
34. Dirk W.C., Inabe T., Schoch K.F. Jr., Marks T.J. *J. Am. Chem. Soc.* **2002**, *105*, 1539.
35. Sirlin C., Bosio L., Simon J. *J. Chem. Soc. Chem. Commun.* **1987**, 379.
36. Konarev D.V., Kuzmin A.V., Faraonov M.A., Ishikawa M., Khasanov S.S., Nakano Y., Otsuka A., Yamochi H., Saito G., Lyubovskaya R.N. *Chem. Eur. J.* **2015**, *21*, 1014.
37. Faraonov M.A., Romanenko N.R., Kuzmin A.V., Konarev D.V., Khasanov S.S., Lyubovskaya R.N. *Dyes Pigm.* **2020**, *180*, 108429.
38. Faraonov M.A., Yudanova E.I., Kuzmin A.V., Khasanov S.S., Troyanov S.I., Otsuka A., Yamochi H., Kitagawa H., Konarev D.V. *CrystEngComm* **2023**, *25*, 4620.
39. Klyamer D., Sukhikh A., Gromilov S., Krasnov P., Basova T. *Sensors* **2018**, *18*, 2141.
40. Schlettwein D., Hesse K., Gruhn N.E., Lee P.A., Nebesny K.W., Armstrong N.R. *J. Phys. Chem. B* **2001**, *105*, 4791.
41. Ouedraogo S., Meunier-Prest R., Kumar A., Bayo-Bangoura M., Bouvet M. *ACS Sensors* **2020**, *5*, 1849.
42. Mirabito T., Huet B., Briseno A.L., Snyder D.W. *J. Cryst. Growth* **2020**, *533*, 125484.
43. Klyamer D.D., Sukhikh A.S., Trubin S.V., Gromilov S.A., Morozova N.B., Basova T.V., Hassan A.K. *Cryst. Growth Des.* **2020**, *20*, 1016.
44. Klyamer D., Bonegardt D., Krasnov P., Sukhikh A., Popovetskiy P., Basova T. *Chemosensors* **2022**, *10*, 515.
45. Bouvet M., Guillaud G., Leroy A., Maillard A., Spirkovitch S., Tournilhac F.-G. *Sens. Actuators, B* **2001**, *73*, 63.
46. Klyamer D., Sukhikh A., Nikolaeva N., Morozova N., Basova T. *Sensors* **2020**, *20*, 1893.
47. Ma X., Chen H., Shi M., Wu G., Wang M., Huang J. *Thin Solid Films* **2005**, *489*, 257.
48. Yutronkie N.J., King B., Melville O.A., Lessard B.H., Brusso J.L. *J. Mater. Chem. C* **2021**, *9*, 10119.
49. APEX3 (v.2019.1-0), Bruker AXS Inc. Madison, Wisconsin, USA, **2019**.
50. Dolomanov O.V., Bourhis L.J., Gildea R.J., Howard J.A.K., Puschmann H. *J. Appl. Crystallogr.* **2009**, *42*, 339.
51. Sheldrick G. M. *Acta Crystallogr. Sect. A Found. Crystallogr.* **2015**, *71*, 3.
52. Sheldrick G. M., *Acta Crystallogr. Sect. C Struct. Chem.* **2015**, *71*, 3.
53. Spackman P.R., Turner M.J., McKinnon J.J., Wolff S.K., Grimwood D.J., Jayatilaka D., Spackman M.A. *J. Appl. Crystallogr.* **2021**, *54*, 1006.
54. Durmuş M., Yeşilot S., Ahsen V. *New J. Chem.* **2006**, *30*, 675.
55. Görlach B., Hellriegel C., Steinbrecher S., Yüksel H., Albert K., Plies E., Hanack M. *J. Mater. Chem.* **2001**, *11*, 3317.
56. Apostol P., Bentaleb A., Rajaoarivelo M., Clérac R., Bock H. *Dalton Trans.* **2015**, *44*, 5569.
57. Rager C., Schmid G., Hanack M. *Chem. Eur. J.* **1999**, *5*, 280.
58. Görlach B., Dachtler M., Glaser T., Albert K., Hanack M. *Chem.Eur. J.* **2001**, *2*, 2459.
59. Nizovtsev A.S. *J. Struct. Chem.* **2022**, *63*, 1491.
60. Ishii K., Kobayashi N. In: *The Porphyrins Handbook. Vol. 16. Phthalocyanines: Spectroscopic and Electrochemical Characterization* (Kadish K.M., Smith K.M., Guilard R., Eds.), Elsevier Science, **2003**. Ch. 102, pp. 1-42.
61. Sukhikh A., Bonegardt D., Klyamer D., Basova T. *Dyes Pigm.* **2021**, *192*, 109442.
62. Sukhikh A., Klyamer D., Bonegardt D., Basova T. *Int. J. Mol. Sci.* **2023**, *24*, 2034.
63. Bonegardt D., Klyamer D., Krasnov P., Sukhikh A., Basova T. *J. Fluor. Chem.* **2021**, *246*, 109780.
64. Zhang Y., Zhang X., Liu Z., Xu H., Jiang J. *Vib. Spectrosc.* **2006**, *40*, 289.
65. Kroenke W.J., Kenney M.E. *Inorg. Chem.* **1964**, *3*, 251.

Received 14.04.2024
Accepted 29.05.2024